Phys Chem Minerals (2003) 30: 393–400
DOI 10.1007/s00269-003-0329-z

ORIGINAL PAPER

E. Fritsch · J. Wéry · G. Jonusauskas · E. Faulques

Transient photoluminescence from highly disordered silica-rich natural phases with and without nanostructures

Received: 25 November 2002 / Accepted: 14 April 2003

Abstract The ultrafast transient photoluminescence of impact silica-rich glasses and nanostructured opals is investigated at the (sub)nanosecond time scale. Spectral and temporal data were acquired with a high-resolution streak camera under high-density energy laser excitation at 4.17 eV (297 nm). All samples reveal blue photoluminescence relaxing in less than 50 ns. Relaxation decays and luminescence energy vary strongly from opals to impact glasses. Opals are found to relax in less than 16 ns with a maximum emission at 2.6–2.8 eV (443–477 nm) while the high-silica glasses exhibit a much longer luminescence in the 50-ns time window, which is spectrally blueshifted towards 3.0–3.5 eV (354–413 nm). Results are interpreted in terms of the presence of nonbridging oxygen atoms, network modifiers, and nanostructures which produce emission from self-trapped excitons and from excitons recombining at surface defects. The short-lived emissions of opals are characteristic of intrinsic surface photoluminescence quenched after about 10 ns via nonradiative decay channels with an annihilation component, and involve recombination luminescence of self-trapped excitons.

Keywords Opal · Tektites · Ultrafast · Photoluminescence · Nanostructure · Excitons

E. Fritsch · J. Wéry · E. Faulques (✉)
Institut des Matériaux Jean Rouxel,
2 rue de la Houssinière,
BP 32229, 44322 Nantes, France
e-mail: faulques@cnrs-imn.fr
Tel: 33–2 40 37 39 77
Fax: 33–2 40 37 39 91

G. Jonusauskas
Centre de Physique Moléculaire Optique et Hertzienne,
Université de Bordeaux I,
351 Cours de la Libération, 33405 Talence, France

Introduction

There is a strong interest in understanding the optophysical properties of SiO_2 and oxidized porous silicon (OPS) because of the technological applications of these oxides in optics and electronics. SiO_2 occurs in a variety of crystalline polymorphs. In particular, natural opals offer the unique opportunity to study micro-to nanostructured hydrated SiO_2 polymorphs with relatively high specific surface area. Depending on their mineralogical origin (volcanic or sedimentary), opals present a wide diversity in their microstructures (Sanders and Murray 1978; Fritsch et al. 1999). They have been classified into a number of categories (Jones and Segnit 1971; Graetsch 1994): the most common are opal A (for amorphous) and opal CT (for cristobalite-tridymite). Opal CT is actually composed of disordered cristobalite crystals with a certain percentage of tridymite stacking (Elzea and Rice 1996). There is also a gemological classification which separates play-of-color noble opal (essentially opal A) from opals without play of color called common opals (predominantly opal CT). Nevertheless, within each opal category or variety the microstructure or texture is reproducible from one sample to the next and yields therefore reliable standards for physical investigations. Indeed, in noble opal there are extensive areas with long-range order and regular stacking of spheres about 200 nm in diameter, this periodic structure being responsible for visible light diffraction (play of color) (Graetsch 1994). On the other hand, common opal is built up of nanograins about 20 nm in diameter (Fritsch et al. 2002) that may be arranged in a number of non-diffracting structures.

By contrast, high-silica glasses (HSG) occurring in nature (impactites, tektites, and obsidians) are totally amorphous and do not contain SiO_2 crystalline polymorphs except in the form of well-segregated inclusions (e.g., millimeter-sized cristobalite spheroids in Lybian desert glass). Because of this lack of intrinsic texture,

their study can be useful for comparing their optical properties with those of textured silica phases.

Optical data, photoluminescence (PL), and absorption spectra of high-silica phases like quartz, silica glass and OPS are relatively well-documented in the literature (Rossman 1994, Song and Williams 1996). However, many of the PL experiments performed on SiO_2 materials used only high-energy excitations, X-rays, 2 MeV electron pulses, or shortwave ultraviolet (UV) up to 10.2 eV (121 nm).

Ultrafast time-resolved PL does not seem to have been investigated systematically to our knowledge in opals and impact high-silica glasses, although this technique can provide much information concerning the temporal evolution of primary excitations and their relationship with nanostructure, network modifiers, and optical properties in general. This lack of data is particularly blatant for high-silica glasses, which are usually described as inert to long-wave ultraviolet radiations, at least when they are of natural origin. In this work, we demonstrate that this is not so and that radiation of high-energy density provided by a picosecond laser in the near-UV range (4.17 eV–297 nm) is able to generate photoluminescence in samples where it was not detected before.

In this paper, we present transient PL data obtained on generic classes of natural materials which have been extensively studied with various techniques in other fields (chemistry and mineralogy). They represent model materials for photoemission studies of silica-rich phases. We show that nanostructure and surface states are relevant to the understanding of the contrasting emissive properties of these materials.

Experimental

Samples investigated were noble opal (opal A) **1**, common opal (opal CT) **2**, Lybian desert glass (LDG) **3**, and moldavite **4** (Table 1). Choice of impact glasses **3** and **4** was made because LDG is richest in silica among naturally occuring glasses such as impactites, tektites, and obsidians, while moldavite is the glass richest in SiO_2 among the class of tektites. Chemical compositions of the four samples are given in Table 1 and are typical of these classes of materials (Bartoli et al. 1990; Rocchia et al. 1996; Faulques et al. 2001).

Time-resolved experiments were carried out at room temperature using a C5680 Hamamatsu streak camera in single-shot mode, with high dynamical range and high time resolution (1.5 ps). The laser setup consists of a hybrid mode-locked dye laser associated with an actively mode-locked continuous wave-pumped Nd:YAG laser, a dye amplifier, and a Nd:YAG regenerative amplifier. The laser system generates pulses of 1 ps (1 mJ, 10 Hz repetition rate) tuned to 2.09 eV (594 nm). The amplified dye laser pulse is frequency-doubled in a KDP type-1 crystal. The excitation energy per pulse at 4.17 eV (297 nm) was 20 μJ with a pulse duration of 1 ps (Dumon et al. 1994). The streak camera was coupled to a monochromator of 0.25 m focal length with a 50 grooves mm^{-1} grating and the emission was recorded in the spectral range 2.07–4.13 eV (300–600 nm) . For each streak image the exposure time was set between 2 and 10 s with 60 to 300 accumulations for each experiment. Both photon counting and analogue integration were chosen for the acquisitions. The images were acquired in reflection geometry with an angle of 20° between the excitation beam and the direction of observation. The beam diameter on the samples was about 500 μm. The spectral resolution, which is actually the size of the laser beam as seen by the streak camera, was 0.06 eV (about 10 nm in that range). Streak images were processed using the HPD-TA Hamamatsu software.

Open specific surfaces were measured using the BET method on a Micromeritics ASAP 2010 instrument (Brunauer et al. 1938), nitrogen being the adsorbed gas.

Results

The streak images (wavelength of emission versus delay after excitation) recorded from the samples in the 2.25–4.13 eV (300–550 nm) spectral range are shown in Fig. 1. In these maps, false colors going from blue to red represent increasing luminescence. All samples have a globally similar spectral character. The emission spectra of these SiO_2 phases share some common features. For all samples the PL is broad and covers almost all the

Table 1 Chemical composition in major oxides percentages of the high-silica materials investigated in this work. Geographical origin as well as structural and optical characteristics are included

Type of material	**1** Play-of-color gray opal A	**2** Common white opal CT	**3** Lybian desert glass, impactite	**4** Moldavite, tektite
Geographical origin	Lightning Ridge, New South Wales, Australia	Mapimi, Mexico	Egypt	Bohemia-Czech Republic
$\%_w$ SiO_2	91.73	92.80	94.8	81.3
$\%_w$ Al_2O_3	0.46	0.31	0.8	9.5
$\%_w$ Fe_2O_3	0.06	0	0.13	1.8
$\%_w$ MgO	0	0.32	0	1.23
$\%_w$ K_2O	0.04	0	0	3.4
$\%_w$ Na_2O	nd	nd	0	0.26
$\%_w$ CaO	nd	nd	0.04	1.75
$\%_w$ TiO_2	0	0	0	0.4
Others	0.2 (mostly Zr, Na, Ca)	0.07 (mostly Zr)	Rb_2O (2%), SrO (1.2%)	Zr, Rb, Sr, Mn
% H_2O	7.5	6.5	Less than 0.1	Less than 0.1
Specific surface	1.2 m^2g^{-1}	3.3 m^2g^{-1}	0.31 m^2g^{-1}	0.37 m^2g^{-1}
SWUV luminescence[a]	Strong blue-white	Strong green	Inert	Inert
XRD	Opal A	Opal CT	Amorphous	Amorphous

[a]With a 4-W classical UV lamp

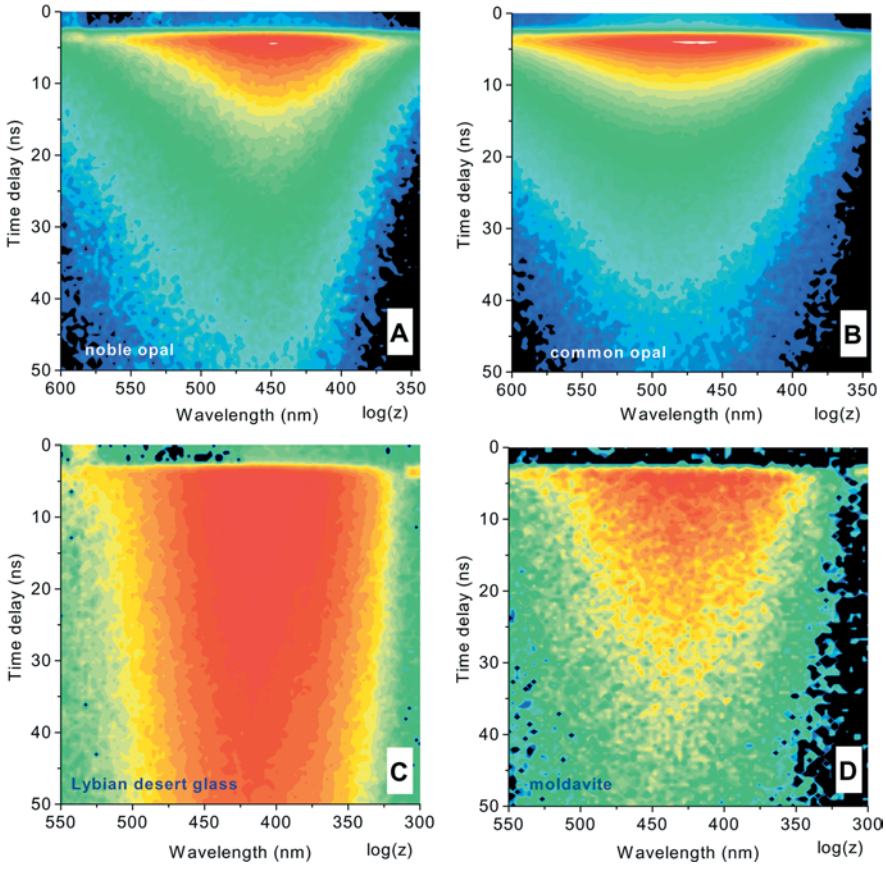

Fig. 1A–D Transient photoluminescence contour maps in false colors of : **A** play-of-color noble A opal-1, **B** common CT opal-2, **C** Lybian desert glass 3, **D** moldavite glass 4. The maps have been integrated on the full time window (50 ns). The intensity z of photoluminescence (PL) is given in logarithmic scale and increases from blue colors to red colors. PL is normalized to the maximum intensity in each case: A 16 000 counts; B 3000 counts; C 1200 counts; D 20 counts. Zero time delay corresponds to the beginning of the streak camera sweep

visible range. They clearly present a delayed luminescence in the 50-ns time window and a maximum emission in the blue-green range. These luminescence characteristics are better seen when spectral and temporal profiles are extracted from the maps, and will be discussed hereafter.

Figures 2 and 3 show the 50-ns integrated PL spectra of the four samples which are fitted with one or two Gaussian profiles. The PL decays are shown in Figs. 2 and 4 for each spectral component. For high-silica glasses (HSG), the emission consists of two superimposed intense components (Fig. 3) at 3 eV (413 nm) and 3.5 eV (354 nm). The emission of LDG is obviously much more intense than that of moldavite, as seen directly from the streak-camera map contour plots (Fig. 1) and the noise level of the spectra (Fig. 3); moreover LDG is found to luminesce under the 1 ps UV-laser excitation with the naked eye while no such observation is possible for moldavite . The luminescence of these two HSG is, however, very similar, since it is composed of two intense "blue"-sided and "red"-sided Gaussian spectral components whose relative energy shift is $\Delta E \approx 0.4$ eV. A careful comparison of the two spectral components of our HSG shows that the "red" emission of moldavite is spectrally broadened by 0.1 eV, while its "blue" emission is spectrally narrowed by 0.06 eV (Fig. 3). The full widths at half maximum (FWHM) of these components are 0.46/0.45 and 0.57/0.37 eV for LDG and moldavite, respectively.

Features of the PL transients of opals are the following : the maximum emission (2.76V–449 nm–FWHM 0.53 eV in 1 and 2.6 eV–477 nm–FWHM 0.59 eV in 2) is noticeably red-shifted with respect to amorphous HSG 3 and 4 (about −0.4 eV) while the relaxation of luminescence is much more rapid (two to six times faster). The spectra of opals can be satisfactorily reproduced with only one Gaussian component, contrasting with the double Gaussian shape of amorphous high-silica glasses.

We notice that the PL bandshapes do not show vibronic components. The absence of vibronic structure indicates that the vibrational relaxation time in SiO_4 tetrahedra is much shorter than the time scale of the experiment. It can be interpreted by the fact that in the nanosecond time range there is no coupling of excitations with intramolecular vibrational degrees of freedom.

Discussion

We discuss first the emissive characteristics of the two HSG samples of this study (3 and 4). The chemical analyses of moldavite and Lybian desert glasses show they are less hydrous than opals, from 0.006 to 0.01% in moldavite, up to 0.14% in LDG, and typically 6 to 9% in opals, in mass percentages (Gilchrist et al. 1969; Frischat et al. 1984; Beran and Koeberl 1997; Holzhey 1997). In contrast to opals, they have poor intermediate- and long-range

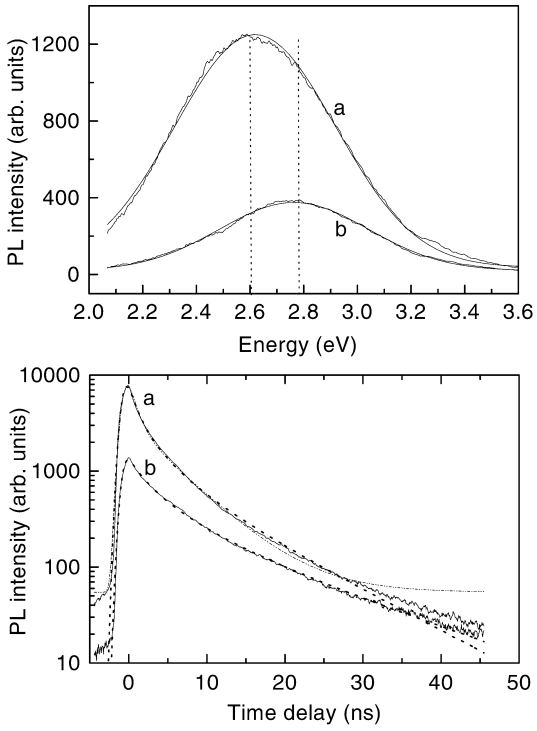

Fig. 2 Transient photoluminescence spectra of opals (*upper panel*) and kinetics of photoluminescence decays (*lower panel*). *a* common CT opal-2; *b* noble A opal-1. Zero time delay has been set to the beginning of decays. The *dashed lines* are the best numerical fits to the data using the annihilation model (Eq .1 including the γn^2 term). The *dash-dotted line in curve a* is an analytical fit to the data of CT opal using a biexponential monomolecular decay (Eq. 2a and b). For noble A opal the fit with the latter model is nearly superposable with that of the former

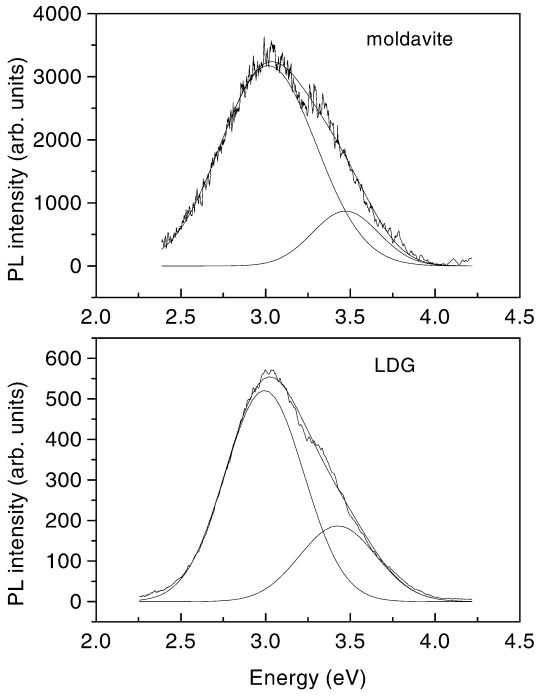

Fig. 3 Transient photoluminescence spectra of Lybian desert glass **3** and moldavite glass **4**. *The two Gaussian peaks* reproducing the spectra are referred to in the text as red-sided and blue-sided components

ordering with no micro- or nanostructures. Finally, these HSG contain elements playing the role of network modifiers such as Al, Fe, or K (Zavetova et al. 1989; Koeberl 1992). In such glassy, high-silica materials, the network modifiers compete substantially with nonbridging oxygen atoms (NBO) occurring from surface defects generated by partial breaking of the Si-O-Si framework. Furthermore, LDG is richer in silica (94–98% SiO_2) than moldavite (typically 80% SiO_2). Moldavite is a glass containing a relatively high proportion of network modifiers (up to 20%) whereas those figures for LDG are considerably lower, a few percent at the most (Koeberl 1986; Faulques et al. 2001). Consequently, the average proportion of NBO atoms occurring from structural defects is higher in the LDG framework than in moldavite, where the NBO population is reduced by the network modifiers. The presence of a low NBO proportion and high concentration of network modifiers in moldavite is clearly to be related to the emission variation between LDG and moldavite and should also account for the different emissive behavior with respect to opals, which are even lower in modifiers than LDG. It has to be noted that these variations should also be related to the particular arrangement of silica nanospheres in opals (Sanders 1980) and of SiO_4 tetrahedra in HSG. At the molecular scale, structural and spectroscopic studies of vitreous silica and natural HSG glasses show that these phases exhibit short-range order consisting of ring structures formed by cyclic arrangements of SiO_4 tetrahedra (T) with 3 to 6 T units bridged by oxygen atoms (Sharma et al. 1981; Galeener 1982; White and Minser 1984). These ring structures can be characterized with Raman spectroscopy. The Raman spectrum of LDG is nearly superposable to that of pure vitreous silica (Faulques et al. 2001), while it differs considerably from that of opals. Thus, we believe that the superimposed components of the emission found in HSG at 3 and 3.5 eV are more likely related to luminescence from defects perhaps in these molecular ring structures than to surface luminescence as discussed below for opals.

For opals, the maximum emissions observed in the transient experiments are very close to those found previously in steady-state continuous wave (cw) PL excited at various energies in the same samples (Fritsch et al. 2001), and in α-quartz, cristobalite, and ultrapure silica glass. In the latter three phases, a strong band at 2.6 eV under 10.2-eV excitation was attributed to intrinsic self-trapped excitons (STE). For α-quartz, luminescence bands at 2.8 eV (443 nm), 3.26 eV (380 nm), and 3.54 eV (350 nm) were also reported, the former also being ascribed to STE excitons (Song and Williams 1996). An STE is an electron-hole pair which localizes itself in the potential well created by its own self-induced lattice distortion. Calculations showed that in cristobalite the STE is a triplet exciton (T) formed by the displacement of the oxygen atom on the Si–O–Si bond with strong localization of hole density onto that

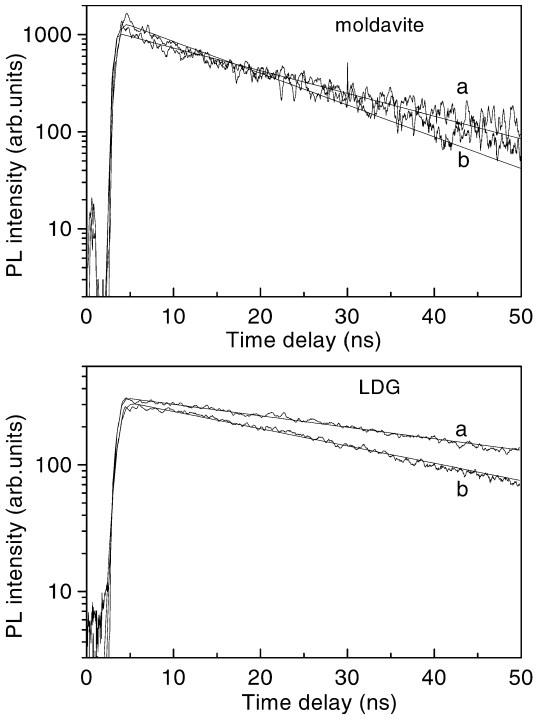

Fig. 4 Kinetics of photoluminescence decays for Lybian desert glass **3** and moldavite glass **4**: *a* Red component ; *b* blue component (see Fig. 3). *Solid lines* are analytical fits to the data using a one-level rate equation with exponential monomolecular decay (Eq. 1 without the γn^2 term). Here, zero time delay corresponds to the beginning of the streak camera sweep

oxygen atom and weaker electron localization on the adjacent Si atom. In amorphous SiO_2, a different local relaxation model has been proposed but the exciton bears the properties of an STE (Song and Williams 1996). In opals we therefore expect that the 2.6–2.8 eV band is mainly due to recombination luminescence of STE. In particular, such an assumption is supported by the fact that CT opal is mainly composed of cristobalite nanocrystals.

The PL blueshift of A opal-1 ($E_{max} = 2.8$ eV–443 nm) compared to that of CT opal-2 ($E_{max} = 2.6$ eV–477 nm) (Fig. 2, upper panel) is 0.2 eV (34 nm). Independently of the nature of the excitations, this spectral shift can be related to the structural difference between the two opals: these materials are characterized by strong porosity with or without cavities in the bulk, increasing dramatically the total specific surface area S_A reached by the radiation with respect to HSG. It is found that $S_A = 3.3\ m^2\ g^{-1}$ in CT opal-2 and $S_A = 1.2\ m^2\ g^{-1}$ in A opal-1 (Fritsch et al. 2001). This difference in S_A arises from the more divided nature of the silica in common CT opal, which is mainly composed of 20-nm nanograins while in play-of-color A opal-1 the spheres of truly amorphous, glass-like material are about 200 nm in diameter (Fritsch et al. 2002). The variation in the maximum emission energy may therefore be related not only to the chemical composition but also to the specific surface area. Assuming that emission is indeed caused by surface processes, since the surface energy per mass unit should be roughly the same in both opal materials due to their nearly identical chemical composition, this qualitatively means that the average energy per surface unit available for radiative processes is less in CT opal-2. This may induce some slight lowering of the electronic energy levels resulting in a red-shifted emission of CT opal-2 with respect to that of play-of-color A opal-1. Surface states may therefore contribute to the PL of noble opal while STE dominate that of CT opal-2. Another spectral difference between the two opals is a very weak additional emission at 3.4 eV (365 nm) found only in A opal-1 at the same energy as the blue-sided, intense component of HSG-3 and −4, which probably characterizes the amorphous texture of this sample. We would like to point out that STE emission and surface emission from defective states are not necessarily antagonist phenomena but could be associated processes. Indeed, excitation spectroscopies and radiation-damage studies have shown in amorphous silica that the STE formation may be approximated to defect pairs of a displaced oxygen atom occupying interstitial sites (as in, e.g., peroxy radicals Si–O–O°) and an E′ center (an unpaired electron on an adjacent Si atom) (Song and Williams 1996).

In the assumption that, besides STE recombination, surface luminescence contributes to the emission of opals, three kinds of NBO defects are possible in these materials which are composed essentially of silica. The first defect consists of a single nonbridging oxygen atom in the SiO_4 tetrahedron. It would be responsible in cooperation with STE for the strong emission found at 2.6 eV (477 nm) in CT opal-2. In the case of two or three nonbridging atoms, the SiO_4 tetrahedron has nearly the vibrational properties of a free SiO_4^{-4} molecule, and therefore strong electron–vibration interaction should be detected in the emission spectra. This is seen indeed for cw PL (Fritsch et al. 2001) but not for transient PL. We conclude that NBO defects of the first kind are probably playing a role in the emission properties of A opal-1.

A previous study (Fritsch et al. 2001) has shown that the cw PL spectra of the same opal samples (1 and 2) reveal a superimposed intense vibronic structure in the spectral range 2–2.6 eV (477–620 nm) ascribed to uranyl ions which are present in opals as extrinsic moieties (less than 1 ppm in A opal-1 and 50 to 150 ppm in common opal-2). In transient PL spectra no such extrinsic structures can be found (Fig. 2) since uranyl luminescence decay times are very long (in the ms range), while the present experiment can probe only the ns time domain. Therefore, the transient spectra should be characteristic of intrinsic ultrafast luminescence: luminophore impurities in the samples do not interfere with surface luminescence. Experiments at such a short time scale are thus highly suitable for probing intrinsic optical phenomena in these materials.

The temporal dynamics of our samples is also rich in information. Concerning its interpretation, we matched

the temporal profiles by using appropriate kinetics-decay analysis. Temporal profiles were fitted with one-level or two-level decay kinetics, respectively. All fits were performed by minimizing χ^2 on a commercial graphic software with analytical expressions or numerically by Runge–Kutta integration using a MATLAB code. The kinetics were modeled on the full temporal scale and take into account the contribution of the apparatus function. In our case, this apparatus function is given by the Gaussian temporal dependence of the laser pulse and the experimental response is a convolution of the silica signal and of the apparatus function. Therefore, we reproduce the kinetics (PL growth and decay) by analytical or numerical integration of the following differential equations. For one level decay we use:

$$\frac{\mathrm{d}n}{\mathrm{d}t} = \frac{I}{\tau_0\sqrt{2\pi}}\exp\left[-\frac{(t-t_0)^2}{2\tau_0^2}\right] - \frac{n}{\tau} - \gamma n^2 \ , \qquad (1)$$

in which the nonlinear term γn^2 is introduced optionally to account for bimolecular annihilation processes (Faulques et al. 2002). For two coupled levels decaying exponentially we fit the temporal signal with:

$$\frac{dn_1}{dt} = \frac{I}{\tau_o\sqrt{2\pi}}\exp\left[-\frac{(t-t_0)^2}{2\tau_0^2}\right] - \frac{n_1}{\tau_1}$$
$$\frac{dn_2}{dt} = \frac{n_1}{\tau_1} - \frac{n_2}{\tau_2} \qquad (2a)$$

In this case, the observed signal is reproduced with the expression:

$$S(t) = A_1 \times n_1(t) + A_2 \times n_2(t) \ , \qquad (2b)$$

with A_1 and A_2 being adjustment parameters where the analytical function $S(t)$ therefore does not involve simple exponentials, but a combination of exponentials with error functions erf(t).

In these equations, t is the time delay, n, n_1, n_2 are the excited state populations, t_0 is the position of the laser pulse maximum in the temporal domain, I its integrated intensity, τ_0 its width, and τ, τ_1, and τ_2 are the monomolecular decay times.

Table 2 summarizes the physical parameters extracted from the fits. From the temporal analysis, it is striking that both blue and red components of the excited-state population of HSG decay perfectly linearly on a semilog scale according to a single exponential law, characterizing unambiguously a single excited level relaxing at times relatively slower than in opals (Fig. 4). The emission therefore clearly proceeds from a monomolecular mechanism. The red component decays about 1.5 times slower than the blue one. In addition, the PL of moldavite-4 decays 2.5 times faster than that of LDG-3. Again, this observation has to be linked with the different proportion of network modifiers in samples 3 and 4. Indeed, a higher amount of network modifiers in sample 4 should favor rapid nonradiative recombination of excitons and quench luminescence by shortening the life of excitations with respect to sample 3.

In the authors' experience, the nearly perfect linear curve (in semilog scales) seen for LDG in Fig. 4 is extremely rare among solids. Usually, there is a slight incurvation, due to minor quenching often related to impurities. This particularly "straight" decay can be explained by the thermally activated recombination of highly mobile electrons and holes trapped onto radiative defects (van Amerongen et al. 2000). Such a mechanism requires that the spatial separation of the trapped charge carriers be small, which most likely occurs for NBO defects.

On the contrary, it is striking from Fig. 2, lower panel, that the excited-state relaxation governing the exciton recombination in opals 1 and 2 is strongly nonexponential. In opals, the PL is so drastically quenched after 1 ns that the probability of nonradiative transitions should increase as time proceeds, while the spectral weight of the emission in HSG is much higher in this temporal domain. Relaxation in opals may apparently obey a biexponential law (Eq. 2a,-b) with $\tau_2 = 8.9\tau_1$ in sample 1 and $\tau_2 = 5.9\tau_1$ in sample 2. However, the applicability of this model is very questionable for CT opal-2 because the fit begins to deviate strongly from the experimental curve at relatively short decay times starting at time delay $t = 15$ ns (Fig. 2, lower panel, curve a, dash-dotted line). On the other hand, fits of the opal data with a model involving both monomolecular recombination and exciton annihilation for a single excited state (Eq. 1) yield much better replicas with parameters τ and γ reported in Table 2. Note

Table 2 Transient photoluminescence emission energies E and lifetimes τ obtained by fitting the decays with Eqs. (1) and (2). Subscripts B and R refer to the blue-sided and red-sided spectral components, respectively (see Fig. 3). ***1*** noble A (play of color) opal; ***2*** common CT opal; ***3*** Lybian desert glass (LDG); ***4*** moldavite glass. HSG : high-silica glasses. Lifetimes τ_1 and τ_2 for opals refer to the depopulation of biexponentially coupled levels for the maximum emission (Eq. 2, see text) while other lifetimes for HSG are determined from the monoexponential, monomolecular decays of the blue- and red-sided spectral components (Eq. 1 without γn^2, see Fig. 4). Finally, the parameters τ and γ obtained for opals are derived from the best fits using the exciton annihilation model (Eq. 1 including γn^2 for bimolecular process).

Sample		E_{max}(eV)	E_B(eV)	E_R(eV)	τ_B(ns)	τ_R(ns)	τ_1(ps)	τ_2(ns)	τ (ns)	γ(ns^{-1})
Opals	**1**	2.76	(3.45)	2.76	–	–	900	8	16.20	0.260
	2	2.60	–	–	–	–	950	5.6	10.47	0.675
HSG	**3**	3.04	3.42	3	32	48	–	–	–	–
	4	3.04	3.47	3.01	13	18	–	–	–	–

that $\tau \sim 2\tau_2$. In CT opal, there is also a slight deviation between the experimental and the calculated decay which starts at $t = 30$ ns (Fig. 2, lower panel, curve a, dashed line). Nevertheless, if the annihilation mechanism contributes significantly to the PL decays, we find that for the two opals the ratio $r = 1/\tau\gamma$ is much less than 1. This substantiates the fact that annihilation predominates over monomolecular recombination. Thus, bimolecular recombination and perhaps more complex processes are probable mechanisms contributing to the exciton luminescence in opals.

Additionally, it is manifest from Table 2 that emissions of opals are at least 1 order of magnitude faster than in HSG. This, associated with the overall spectral blue shift of the maximum emission in HSG strongly suggests again that the emission of opal is a comparatively more complex process, partly dominated by non-radiative recombination mechanisms and possibly involving exciton triplet annihilations (e.g., STE).

Since opals contain more than 5% water, it is likely that the rapid luminescence quenching with respect to HSG proceeds also from complexed water molecules by vibrational losses. Another interesting observation is the peculiar red shift of the PL contour plots of CT opal-2 (≈ 0.07 eV or 13 nm or 580 cm^{-1}) when the time delay increases (Fig. 5). This may be typical of triplet states like STE since triplets are on lower energy levels than singlet states. It indicates a probable migration of some fraction of STE excitons recombining onto non-radiative traps. Further, the lifetime τ and the annihilation rate γ of A opal-1 are respectively higher and lower (16.2, 0.26 ns^{-1}) than those of CT opal (10.5, 0.67 ns^{-1}). This is strong evidence that PL quenching is more efficient in CT opal.

We note that an interesting energy-transfer model between acceptor and donor fluorescent molecules has been proposed to probe the pore morphology of synthetic porous silicas by means of transient photoluminescence experiments (Klafter and Blumen 1985; Levitz and Drake 1987). The decay curves reported in the latter reference refer to the emission of donor (rhodamine 6G) and acceptor (malachite green) molecules adsorbed in the silica pores. Possibly, if such molecules could be embedded in opals, their pore morphology would be probed as well with this technique.

Finally, scanning electron microscopy (SEM) and atomic force microscopy (AFM) imaging show that the structure of CT opal is formed with nanograins of 20 nm in size while that of noble opal consists of spheres of 150–200 nm in size (Fritsch et al. 2002). We can estimate the intermolecular diffusion constants D_c of the excitations in opals with the following simple relationship:

$$D_c = \frac{R^2}{\tau} \quad , \tag{3}$$

where R is the domain size (200 or 20 nm) traveled by the excitation and taking for τ the lifetime deduced from the annihilation model. We find $D_c = 3.8 \times 10^{-4}$ cm^2 s^{-1} for common opal-2 and 2.5×10^{-2} cm^2 s^{-1} in A opal-1. This broad estimate confirms that excitations survive longer in noble opal due to larger domain sizes.

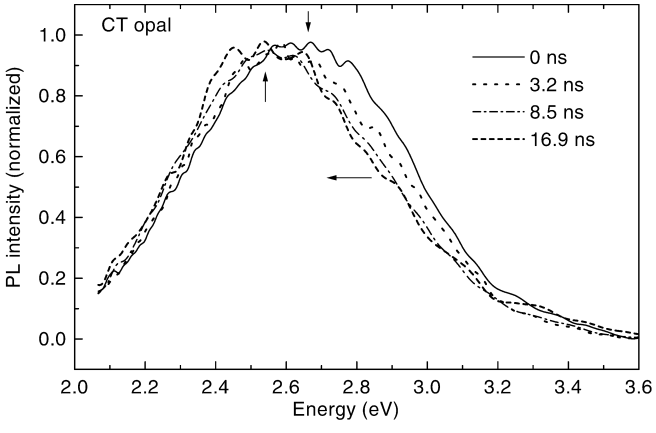

Fig. 5 Spectral shots of the transient photoluminescence of CT opal-2 for increasing time delays after the laser impulsion. As time evolves, the maximum emission and the high-energy wing of the profile are substantially shifted toward lower wavelengths (the red shifts are, respectively, 0.072 eV and 0.067 eV)

Conclusion

In this paper we have reported on the transient emission spectra of highly disordered natural silica phases obtained on four representative samples in the nanosecond time domain. We have found that the transient photoluminescence of opals presents a single band at 2.6–2.8 eV (443–477 nm) while that of high-silica glasses consists of two broader, superimposed components blue-shifted at 3.0–3.5 eV (354–413 nm). Vibronic lines are not observed in this kind of experiment, in contrast to steady-state measurements. The different emissive behavior between opals and high-silica glasses in the spectral and temporal domains is ascribed to (1) surface luminescence of excitons recombining at nonbridging oxygen defects and (2) self-trapped excitons. In both opals the photoluminescence is strongly quenched after 1 ns. A law including annihilation of excitons reproduces apparently well their emission decays. In high-silica glasses the excitons recombine according to a pure exponential relaxation and survive over 50 ns. These different mechanisms have to be related to a higher proportion of non-bridging oxygen surface defects in opal and a higher proportion of network modifiers present in the high-silica glasses.

References

Bartoli F, Bittencourt RD, Doirisse M, Meyer R, Philippy R, Samama JC (1990) Role of aluminum in the structure of Brazilian opals. Eur J Mineral 2: 611–619

Beran A, Koeberl C (1997) Water in tektites and impact glasses by Fourier-transform infrared spectroscopy. Meteorit Planet Sci 32: 211–216

Brunauer S, Emmett PH, Teller E (1938) Adsorption of gas in multimolecular layers. J Am Chem Soc 60: 309–319

Dumon P, Jonusauskas G, Létard JF, Pée Ph, Dupuy F, Lapouyade R, C.Rullière C, (1994) Picosecond dynamics of cation–macrocycle interactions in the excited state of an intrinsic fluorescence probe: the calcium complex of 4-(N-monoaza-15–crown-5)-4'-phenyl stilbene. J Phys Chem 98: 10391–10396

Elzea JM, Rice SB (1996) TEM and X-ray diffraction evidence for cristobalite and tridymite stacking sequences in opal. Clays Clay Miner 44: 492–500

Faulques E, Fritsch E, Ostrooumov M (2001) Spectroscopy of natural silica-rich glasses. J Mineral Petrol Sci 96: 120–128

Faulques E, Wéry J, Lefrant S, Ivanov VG, Jonusauskas G (2002) Transient photoluminescence of para-hexaphenyl layers. Phys Rev, (B) 65: 212202–1-212202–4

Frischat GH, Klöpfer C, Beier W, Weeks RA (1984) Some properties of Libyan desert glasses. J Non-Cryst Solids 67: 621–628

Fritsch E, Rondeau B, Ostrooumov M, Lasnier B, Marie AM, Barrault A, Wery J, Connoué J, Lefrant S (1999) Découvertes récentes sur l'opale. Rev Gemmol. AFG 138–139: 34–40

Fritsch E, Mihut L, Baibarac M, Baltog I, Ostrooumov M, Lefrant S, Wéry J (2001) Luminescence of oxidized porous silicon: surface-induced emissions from disordered silica micro- to nano-textures. J Appl Phys 90: 4777–4782

Fritsch E, Ostrooumov M, Barreau A, Albertini D, Marie AM, Lasnier B, Wéry J (2002) Mexican gem opals: nano- and microstructure, origin of colour and comparison with other common opals of gemological significance. Aust Gemmol 21: 230–233

Galeener FL (1982) Planar rings in vitreous silica. J Non-Cryst Solids 49: 53–62

Gilchrist J, Thorpe AN, Senftle FE (1969) Infrared analysis of water in tektites and other glasses. J Geophys Res 74: 1475–1483

Graetsch H (1994) Structural characteristics of opaline and microcrystalline silica minerals. In: Heaney PJ, Prewitt CT, Gibbs GV (eds) Silica physical behavior, geochemistry and materials applications. P Ribbe ed. Reviews in Mineralogy. Mineralogical Society of America, Washington DC, pp 209–232

Holzhey G (1997) Feueropal von Opal Butte, Oregon, USA. Z Dtsch Gemmol Ges 46: 161–168

Jones JB, Segnit ER (1971) The nature of opal, part 1. Nomenclature and constituent phases. J Geol Soc Aust 18: 57–68

Klafter J, Blumen A (1985) Direct energy transfer in restricted geometries. J Luminescence 34: 77–82

Koeberl C (1986) Geochemistry of tektites and impact glasses. Annu Rev Earth Planet Sci 14: 323–350

Koeberl C (1992) Geochemistry and origin of Muong Nong-type tektites. Geochim Cosmochim Acta 56: 1033–1064

Levitz P, Drake JM (1987) Direct energy transfer in restricted geometries as a probe of the pore morphology of silica. Phys Rev Lett 58: 686–689

Rocchia R, Robin E, Fröhlich F, Méon H, Froget L, Diemer E (1996) L'origine des verres lybiques: un impact. CR Acad Sci Sér 2 Sci Terre Planètes 32: 839–845

Rossman GR (1994) Colored varieties of the silica minerals In: Heaney PJ, Prewitt CT, Gibbs GV (eds) Silica physical behavior, geochemistry and materials applications. P Ribbe ed. Reviews in Mineralogy. Mineralogical Society of America, Washington DC pp 433–468

Sanders JV, Murray MJ (1978) Ordered arrangements of spheres of two different sizes in opal. Nature 275: 201–203

Sanders JV (1980) Closed-packed structures of spheres of two different sizes. I. Observations on natural opal. Phil Mag (A) 42: 705–720

Sharma SK, Mammine JF, Nicol MF (1981) Raman investigation of ring configuration in vitreous silica. Nature 292: 140–141

Song KS, Williams RT (1996) Self-trapped excitons, 2nd ed Springer, Berlin Heidelberg New York, pp 271–299

van Amerongen H, Valkunas L, van Grondelle R (2000) Photosynthetic excitons. World Scientific, Singapore, p. 22

White WB, Minser DG (1984) Raman spectra and structure of natural glasses. J Non-Cryst Solids 67: 45–59

Zavetova M, Pacesova S, Simeckova M, Schmidt E, Navratil K (1989) Optical properties of natural glasses-moldavites. J Non-Cryst Solids 108: 294–300